Measurement of evaporation residue excitation functions for the ^{19}F + ^{194,196,198}Pt reactions

Varinderjit Singh,* B. R. Behera,† Maninder Kaur, A. Kumar, and K. P. Singh
Department of Physics, Panjab University, Chandigarh 160014, India

N. Madhavan, S. Nath, J. Gehlot, G. Mohanto, A. Jhingan, Ish Mukul, and T. Varughese
Inter University Accelerator Centre, New Delhi 110067, India

Jhilam Sadhukhan
Department of Physics and Astronomy, University of Tennessee, Knoxville, Tennessee 37996, USA
and Physics Division, Oak Ridge National Laboratory, Oak Ridge, Tennessee 37831, USA

Santanu Pal
CS-6/1, Golf Green, Kolkata 700095, India

S. Goyal
Department of Physics and Astrophysics, Delhi University, Delhi 110007, India

A. Saxena, S. Santra, and S. Kailas
Nuclear Physics Division, Bhabha Atomic Research Centre, Mumbai 400085, India
(Received 17 November 2013; published 18 February 2014)

Experimental measurements of evaporation residue (ER) cross sections for the ^{19}F + ^{194,196,198}Pt reactions forming ^{213,215,217}Fr compound nuclei are reported. The cross sections are measured at beam energies in the range of 101–137.3 MeV. The survival probability of the ^{213}Fr compound nucleus with neutron number $N = 126$ is found to be lower than the survival probabilities of ^{215}Fr and ^{217}Fr with neutron numbers $N = 128$ and 130 respectively. Statistical model analysis of the ER cross sections show that an excitation energy dependent scaling of the finite-range rotating liquid drop model fission barrier is necessary to fit the experimental data. The fitted scaling factors for ^{213}Fr are found to be smaller than those of ^{215}Fr and ^{217}Fr for almost the entire range of excitation energies.

DOI: 10.1103/PhysRevC.89.024609 PACS number(s): 25.70.Gh, 24.10.Pa, 25.70.Jj

I. INTRODUCTION

Stability of heavy nuclei against fission is a topic of considerable interest in contemporary nuclear physics research. The main reason for this interest is the possibility of synthesizing superheavy elements (SHE), which are predicted to be stable due to shell effects [1]. It is predicted that the next neutron shell closure after $N = 126$ will be at $N = 184$ and it is expected that this neutron shell closure will be a contributing factor for the stability of a SHE in the mass region $A \sim 300$. It thus becomes important to know to what extent shell closure contributes to the stability of a heavy nucleus against fission. Though shell closure effects give rise to fission barriers typically of the order of a few MeV, the above question arises because other nuclear properties such as the level density and the ground-state deformation can also influence the fission process in addition to the fission barrier. The above issues have been addressed in a number of publications where stability of nuclei near $N = 126$ has been considered [2–7].

Stability against fission of heavy nuclei has been investigated by analyzing experimental data on both fission and evaporation residue (ER) cross sections from heavy-ion-induced fusion-fission reactions and also from isotopic distributions of the production cross sections of various elements in high-energy heavy-ion fragmentation experiments [2–5]. It was shown in Ref. [5] that shell stabilization near $N = 126$ is lost to a great extent due to the collective excitation of level density (CELD) in the actinide region though the effect reduces for nuclei with lower atomic numbers. However, no CELD effect was noticed in a detailed analysis of fission and ER cross sections of polonium isotopes with neutron numbers up to $N = 126$ [4]. The ER cross sections of ^{213}Fr and ^{217}Fr compound nuclei populated in ^{19}F + ^{194,198}Pt reactions were measured earlier up to excitation energies of 60 MeV [3]. The ER cross sections for ^{213}Fr were found to be considerably smaller than those of ^{217}Fr.

In the present paper, we report experimental measurement of ER cross sections of the compound nuclei ^{213,215,217}Fr formed in ^{19}F + ^{194,196,198}Pt fusion-fission reactions. The ER cross sections are measured for excitation energies up to 90 MeV. The main motivation for this work is to search for shell stabilization effect, or the lack of it, for neutron shell closure at $N = 126$. To this end, we compare the measured excitation functions of ER cross section of ^{213}Fr ($N = 126$)

*Present address: GSI Helmholtzzentrun für Schwerionenforschung GmbH, 64291 Darmstadt, Germany.
†Corresponding author: bivash@pu.ac.in

with those of ^{215}Fr ($N = 128$) and ^{217}Fr ($N = 130$) compound nuclei. The present work thus extends the ER cross-section measurement to a larger number of nuclei with $N \geqslant 126$ and to a broader range of excitation energies in comparison to the earlier works [3,4]. We further perform statistical model calculations to analyze the data.

The paper is organized as follows. The details of the experimental set up are given in the next section. The data analysis is given in Sec. III, where the experimental results are also presented. Section IV contains the statistical model analysis of the data. A summary of the work and the conclusions are given in the last section.

II. EXPERIMENTAL SETUP

The experiment was carried out at the HYbrid Recoil mass Analyzer (HYRA) using the 15 UD Pelletron + LINAC accelerator system at Inter University Accelerator Centre (IUAC), New Delhi. Thin isotopically enriched targets of ^{194}Pt, ^{196}Pt, and ^{198}Pt with thicknesses of 265, 170, and 170 μg/cm^2 respectively [8] were bombarded with a pulsed beam of ^{19}F (pulse separation of 4 μs) with an energy range from 101 to 137.3 MeV. The targets were kept at the centre of a scattering chamber of 12 cm diameter. Two Si surface barrier detectors were mounted at a distance of 2.4 cm from the target position, making angles of $\pm 23^\circ$ with respect to the beam direction for monitoring and normalization of the beam flux incident on the target.

The evaporation residues populated during the reaction were separated from beam background using the HYRA spectrometer [9,10]. HYRA is a dual-mode, dual-stage spectrometer with its first stage capable of operating in gas-filled mode in normal kinematics and both stages in vacuum mode in inverse kinematics. In the present study, the first stage of HYRA was operated in gas-filled mode [9]. The gas-filled region was separated from the beam line vacuum using a 1.3 mg/cm^2 rolled self-supporting Ni foil, placed at the entrance of the target chamber. In the gas-filled mode, the ERs undergo multiple collisions with the gas atoms, which result in the change of charge state and hence energy of the ERs. After a number of collisions, the ERs attain a mean charge state, which can be calculated using the empirical formula [11]. The magnetic fields of each magnetic dipole were calculated using the mean charge state and the energy of the ERs at the centre of the dipole. The energy loss of the ERs in the gas medium was also taken into account. The field values of the quadrupole magnets were obtained by scaling the fields of the magnetic dipoles. The values obtained were varied to $\pm 10\%$ in steps of 2% from the calculated values, for optimizing the field setting (this is achieved by maximizing the ratio of ER to monitor yield). The magnetic field optimization was carried out at each energy. At the beginning of experiment, the He gas pressure optimization was also carried out by varying it from 0.10 Torr to 0.25 Torr in steps of 0.05 Torr to maximize the ratio of the ER to monitor yield. The optimum gas pressure was found to be 0.15 Torr, which was kept fixed during the entire experiment.

The focal plane of the HYRA contains a multi wire proportional counter (MWPC) with an active area of 152.4 $\times$ 50.8 mm^2 followed by a two-dimensional position-sensitive Si strip detector with an active area of 50 $\times$ 50 mm^2. The MWPC was operated at 2 mbar pressure of isobutane gas. The isolation between the He gas-filled region of HYRA and the focal plane was made by using a mylar foil of 0.5 μm thickness. The MWPC used at the focal plane was a five-electrode detector (two cathode, two position wire frame and an anode). The MWPC provided position information (both X and Y), a timing signal from the anode, and the information about the energy deposited by the ERs, obtained using the cathode signal. The position signals were taken from the both ends of the X and Y wired frames using delay line chips. A time to amplitude (TAC) spectrum was generated using the MWPC anode as start and the rf of the beam as stop. A two-dimensional spectrum was generated using the TAC and the energy loss of evaporation residues (ERs) (cathode of MWPC), as shown in Fig.1. It provided a clean separation of the ERs from the beam and target contaminations. Due to the low energy of the ERs only a few events were reaching the strip detector. Hence, for the present measurements, only the MWPC detector was used. The details of data analysis are given in the next section.

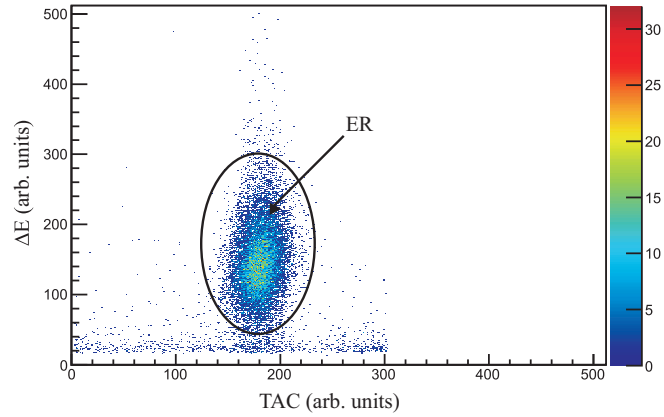

FIG. 1. (Color online) Two-dimensional spectrum of TAC vs MWPC cathode (ΔE) signals.

III. DATA ANALYSIS

For the determination of cross section with the gas-filled separtor HYRA, the knowledge of the various ER channels, its angular acceptance, energy distribution, and transmission efficiency of HYRA is required. The various steps used for obtaining these values for the determination of ER cross sections are described in the following subsections.

A. Evaporation residue channels

Standard statistical model predictions for population of various evaporation residue channels are obtained. It is observed that at low energies, xn channels are the dominant decay modes, whereas at higher energies α channels also start competing with the xn channels. It is observed that all the ERs expected to be populated in the reactions under study have lifetimes greater than the time required by the ERs to reach the focal plane detector (3–4 μs). Hence, it confirms that no ER is decaying before reaching the focal plane.

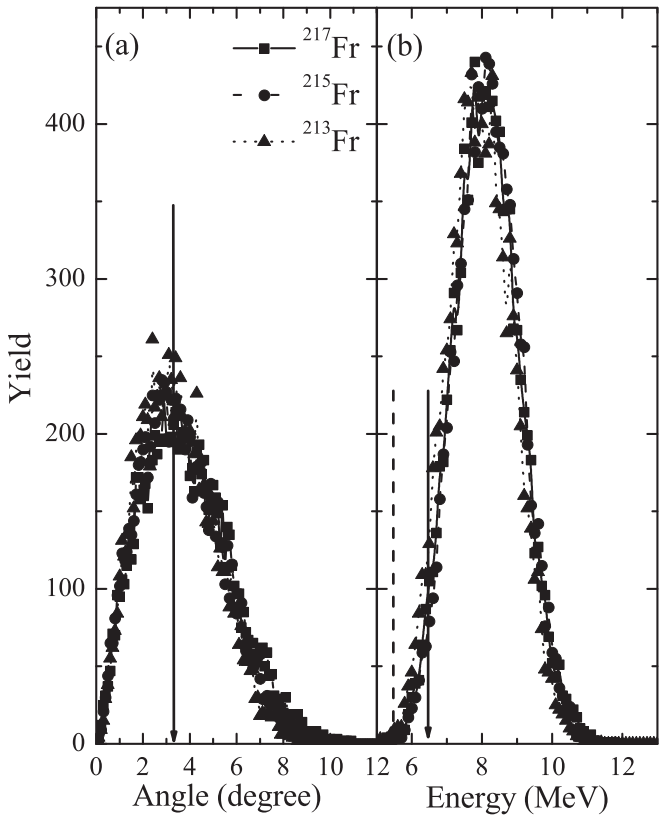

FIG. 2. (a) Angular distributions of ERs obtained by TERS code at 96.6 MeV for the different reactions under study. The vertical line at 3.35° indicates the HYRA angular acceptance. (b) Energy distributions of ERs obtained by TERS code at 96.6 MeV for the different reactions under study. The vertical solid line (6.5 MeV) and dashed line (5.5 MeV) indicate the threshold ER energy for ^{213}Fr and ^{215,217}Fr respectively.

B. HYRA angular acceptance

The distance of the target from the HYRA entrance was 145 mm with 17-mm aperture of HYRA. The angular acceptance of HYRA is found to be ±3.35° with respect to the beam axis. The angular distributions for the reactions at different energies are simulated using the semimicroscopic Monte Carlo simulation code TERS [12]. TERS generates the realistic distribution of ER parameters such as displacement, angular distribution, charge distribution, and energy distribution in event-by-event mode. The TERS calculation considers one ER channel at a time and hence calculations are carried out separately for all the Statistical model predicted ER channels. The total ER angular distribution at each energy was constructed by adding ER angular distributions of individual channels with proper weight. The angular distributions thus obtained for compound nuclei under study at the lowest energy are shown in Fig. 2(a).

C. Evaporation residue energy distribution

All the ERs produced in a reaction do not have the same kinetic energy because of energy loss in the target. The ER energy follows a Gaussian distribution with peak at the mean energy of the ERs. At low beam energies, it is possible that some of the low-energy ERs may stop before reaching the focal plane detector. The energy distribution of ERs is also studied using the TERS code to estimate the percentage of ERs stopping in He before reaching the focal plane. For this estimation, a threshold energy (the minimum energy which the ERs should have to reach and get detected in the focal plane detector) of the ERs is calculated. In these calculations, the ER energy loss in the target thickness, He gas, and Mylar foil are taken into account. It is observed that the threshold ER energies are 5.5, 5.5, and 6.5 MeV for the reactions populating ^{217}Fr, ^{215}Fr, and ^{213}Fr respectively. Figure 2(b) shows the ER energy distributions obtained by the TERS code for all the reactions at the lowest beam energy. It is observed that for the reaction populating ^{213}Fr at the lowest energy, 5% of the ERs are stopping in He gas, and this number drops to 0.5% at the highest energy. However, for the other two reactions, less than 0.5% of the ERs are stopped in He gas at the lowest beam energy and none at higher energies. The ER yields are accordingly corrected to compensate for the ERs stopped in He gas.

D. Evaporation residue cross section

The total ER cross sections can be calculated from the ERs (Y_{ER}) and monitors (Y_{Mon}) yields using the following expression;

$$\sigma_{ER} = \frac{Y_{ER}}{Y_{Mon}} \Omega_{Mon} \frac{d\sigma}{d\Omega_{Mon}}(\theta_{Mon}) \frac{1}{\eta_{HYRA}}, \quad (1)$$

where σ_{ER} is ER cross section, Ω_{Mon} is the solid angle subtended at the monitor detector, η_{HYRA} is the transmission efficiency of HYRA, and $\frac{d\sigma}{d\Omega_{Mon}}(\theta_{Mon})$ is the Rutherford scattering cross section at θ_{Mon}, given as

$$\frac{d\sigma}{d\Omega_{Mon}}(\theta_{Mon}) = \left(\frac{Z_1 Z_2 e^2}{4E}\right)^2 \frac{1}{[\sin(\theta_{Mon}/2)]^4}. \quad (2)$$

The Y_{ER} and Y_{Mon} are obtained from the experimental data, and the relative ER cross sections for the reactions under study are obtained using the following expression:

$$\sigma_{ER}^{rel} = \frac{Y_{ER}}{Y_{Mon}} \Omega_{Mon} \frac{d\sigma}{d\Omega_{Mon}}(\theta_{Mon}). \quad (3)$$

The transmission efficiency of HYRA is required to obtain the absolute ER cross sections. The method used for obtaining the transmission efficiency is described in the next subsection.

E. Transmission efficiency of HYRA

The transmission efficiency is defined as the ratio of the number of ERs reaching the focal plane to the total number of ERs produced. The transmission efficiency mainly depends on the angular acceptance of HYRA and the energy of the ERs produced in a reaction. In order to estimate the transmission efficiency, measurements were performed for ^{19}F + ^{198}Pt and ^{194}Pt systems at the two lowest beam energies, for which the ER cross sections were measured earlier [3]. The transmission efficiency (η_{HYRA}) is obtained by substituting the measured

ER cross sections in the following expression:

$$\eta_{\mathrm{HYRA}} = \frac{Y_{\mathrm{ER}}}{Y_{\mathrm{Mon}}}\Omega_{\mathrm{Mon}}\frac{d\sigma}{d\Omega_{\mathrm{Mon}}}(\theta_{\mathrm{Mon}})\frac{1}{\sigma_{\mathrm{ER}}}. \quad (4)$$

The values of η_{HYRA} obtained are 1.10 ± 0.11 and 1.09 ± 0.09 (all in %) for ^{217}Fr and ^{213}Fr respectively. Since the angular and energy distributions of the systems under study are nearly same as shown in Fig. 2, the η_{HYRA} values obtained from ^{217}Fr and ^{213}Fr can be employed to obtain the same for ^{215}Fr.

In an alternative approach to obtain η_{HYRA}, it is observed that the angular and energy distribution of the systems under study are nearly same to those of the $^{16}\mathrm{O} + ^{194}\mathrm{Pt}$ system. The ER cross sections for $^{16}\mathrm{O} + ^{194}\mathrm{Pt}$ system were measured earlier using the HYRA spectrometer [13]. The only difference from the present experiment was that the size of scattering chamber was larger (angular acceptance of HYRA was more) in earlier work. Hence, the η_{HYRA} obtained for $^{16}\mathrm{O} + ^{194}\mathrm{Pt}$ can be used to obtain the η_{HYRA} for the systems under study by using the proper normalization of angular acceptance. The η_{HYRA} of $^{16}\mathrm{O} + ^{194}\mathrm{Pt}$ system is normalized with the angular acceptance obtained from the weighted average angular distributions using TERS calculations for the reactions under study. The η_{HYRA} values at the lowest energy are 1.033 ± 0.16, 1.0158 ± 0.15, and 0.97 ± 0.147 (all in %) for the ^{217}Fr, ^{215}Fr, and ^{213}Fr compound nuclei respectively. The η_{HYRA} values obtained from both of the above prescriptions match within error bar. Hence any one of these can be used for obtaining the ER cross sections. The η_{HYRA} obtained by the second method is used in the present study.

The η_{HYRA} values at higher energies are obtained using η_{HYRA} values thus obtained at the lowest beam energy. The angular acceptance decreases with increase in the beam energy, which results in the decrease of η_{HYRA}. Hence the η_{HYRA} at the lowest energy is normalized with angular acceptance at higher energies, in order to obtain the η_{HYRA} for higher energies.

F. Experimental results

The transmission efficiencies at different energies are used in Eq. (1) to obtain the ER cross sections. The measured ER cross sections for the different systems under study are shown in Fig. 3 and are also given in Table I. The errors in the measured cross sections include contributions from the statistical error and also the error in η_{HYRA}. It is observed that the ER cross sections of ^{213}Fr are substantially smaller than those of ^{215}Fr and ^{217}Fr, which are of comparable magnitudes.

IV. STATISTICAL MODEL CALCULATIONS

The experimentally obtained ER cross sections are compared here with the statistical model predictions of the decay of a compound nucleus. In the present calculations, emission of light particles (α, neutron, proton), giant dipole resonance (GDR) γ rays and fission are considered as the possible decay channels of the compound nucleus (CN). The decay widths of the light particles and the GDR γ rays are obtained from the Weisskopf formula [14]. The experimental nuclear masses are used to calculate the particle separation energies in the particle decay width calculations. The fission width is taken

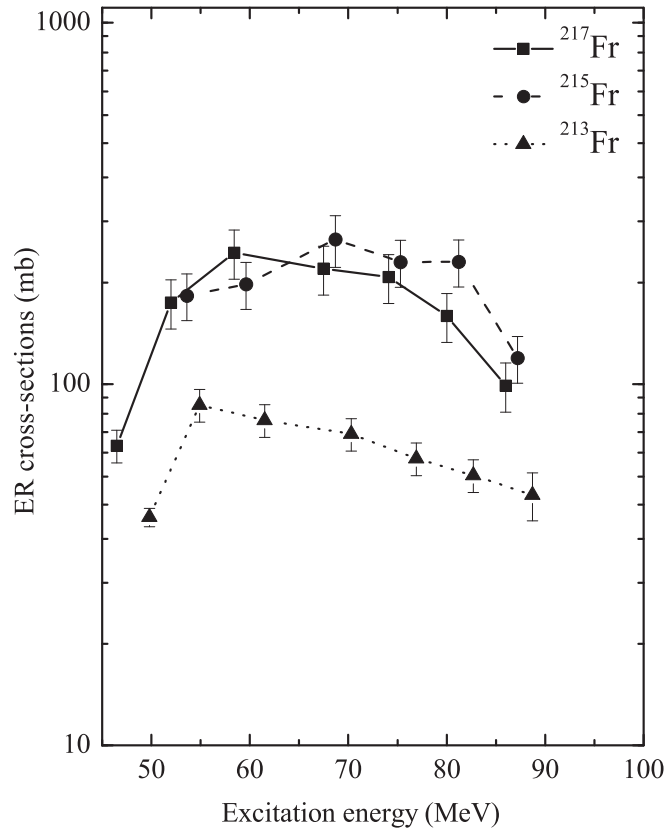

FIG. 3. The excitation function of ER cross sections for different isotopes of Fr. ER cross sections at the lowest energy for ^{213}Fr and ^{217}Fr are taken from the measurement by Mahata *et al.* [3]. The lines are drawn to guide the eye.

from the transition-state model of Bohr and Wheeler and is given as [15]

$$\Gamma_{\mathrm{BW}} = \frac{1}{2\pi\rho_{gs}(E_i)}\int_0^{E_i - V_B}\rho_{\mathrm{sad}}(E_i - V_B - \varepsilon)d\varepsilon, \quad (5)$$

where ρ_{gs} and ρ_{sad} are the level densities at the ground state and the saddle configurations respectively. We further multiply the Bohr-Wheeler width with the phase-space factor $\hbar\omega_{gs}/T$ which takes into account the collective degrees of freedom in the ground state [16]. Here ω_{gs} denotes the frequency of a harmonic oscillator potential having the same curvature as the nuclear potential at the ground state while T represents the nuclear temperature. The competition between the different decay widths decides the fate of a decaying CN.

The nuclear level density is an important ingredient which decides the intensity of different decay modes and is given as [17]

$$\rho(E,l) = \frac{2l+1}{24}\left(\frac{\hbar^2}{2I}\right)^{\frac{3}{2}}\sqrt{a}\frac{\exp(2\sqrt{aE^*})}{(E^*)^2}, \quad (6)$$

where E^*, l, and I are the nuclear excitation energy, spin, and the moment of inertia respectively and a is the level density parameter. The level density parameter is taken from the work of Ignatyuk *et al.* [18], who proposed a form which includes the shell effects at low excitation energies and goes over to its

TABLE I. Measured ER cross sections (in mb) obtained for ^{217}Fr, ^{215}Fr and ^{213}Fr compound nuclei (E^* is the excitation energy).

$E_{\rm Lab}$ (MeV)	E^* (MeV)	^{217}Fr	$E_{\rm Lab}$ (MeV)	E^* (MeV)	^{215}Fr	$E_{\rm Lab}$ (MeV)	E^* (MeV)	^{213}Fr
90.1[a]	46.5	67.5 ± 7.0				90.6[a]	49.8	42.8 ± 4.0
96.5	52.3	168.1 ± 26.1	96.5	53.6	175.7 ± 26.0	96.2	54.9	82.2 ± 12.5
103.1	58.4	230.9 ± 35.9	103.1	59.6	188.8 ± 28.1	103.4	61.5	89.8 ± 13.6
113.1	67.5	208.5 ± 32.3	113.1	68.7	275.8 ± 41.1	113.1	70.3	102.9 ± 15.6
120.3	74.1	197.6 ± 30.6	120.3	75.3	217.6 ± 32.3	120.3	76.9	75.9 ± 11.5
126.8	80.0	154.2 ± 23.9	126.8	81.2	217.9 ± 32.3	126.7	82.7	54.6 ± 8.3
133.4	86.0	98.9 ± 15.3	133.4	87.2	118.0 ± 17.4	133.3	88.7	49.3 ± 7.5

[a]Measurements carried out by Mahata *et al*. [3].

asymptotic form at high excitation energies. It is given as

$$a(E^*) = \overline{a}\left(1 + \frac{f(E^*)}{E^*}\delta W\right) \tag{7}$$

with

$$f(E^*) = 1 - \exp(-E^*/E_d), \tag{8}$$

where $\overline{a}$ is the asymptotic level density and E_d is the parameter which decides the rate at which the shell effects disappear with increase in the excitation energy (E^*). A value of 18.5 MeV is used for E_d which was obtained from analysis of s-wave neutron resonances [19]. The shell correction term δW is given as the difference between the experimental and liquid-drop model (LDM) masses ($\delta W = M_{\rm exp} - M_{\rm LDM}$). The asymptotic level density $\overline{a}$ depends on nuclear shape and is taken from Ref. [19].

The spin distribution of compound nuclei formed in a fusion reaction is required for statistical model calculations. In the present study, the compound nuclear spin distribution is obtained by fitting the experimental fusion cross sections with coupled channel calculations using the code CCDEF [20]. The fission and ER cross sections for the ^{19}F + ^{194}Pt and ^{198}Pt reactions at low excitation energies were measured earlier by Mahata *et al*. [3]. The fusion cross sections at low excitation energies above the Coulomb barrier are fitted with the CCDEF code using the nuclear potential depth and curvature as free parameters. The same parameter sets are used to obtain the fusion cross sections and the spin distributions at higher excitation energies. For the ^{19}F + ^{196}Pt reaction for which experimental fusion cross sections are not available, the CCDEF predicted spin distributions are obtained using the parameter set used for the ^{19}F + ^{198}Pt reaction. The fusion cross sections obtained from CCDEF along with the experimental ER cross sections are shown in Fig. 4.

We next obtain the experimental survival probability as the ratio of the experimental ER cross sections and the CCDEF predicted fusion cross-sections for all the Fr isotopes under study [see Fig. 5(a)]. It is observed that the survival probability of all the isotopes decreases with increase in excitation energy, as expected. However, the survival probability is substantially smaller for the closed-shell CN ^{213}Fr compared to the other two non-closed-shell nuclei,^{217}Fr and ^{215}Fr, which are of comparable magnitudes. This finding is contrary to the expectation that a closed-shell nucleus should be more stable against fission compared to the neighboring non-closed-shell nuclei. The ratio of the survival probabilities of ^{217}Fr and ^{215}Fr with respect to ^{213}Fr are also obtained and are shown in Fig. 5(b). It is observed that the survival probability of both ^{217}Fr and ^{215}Fr with respect to that of ^{213}Fr increases with increase of excitation energy.

We now compare the above trends in the survival probability of the Fr nuclei with the predictions of statistical model calculations. The finite-range rotating liquid drop model (FRLDM) potential is first used to calculate the fission barriers [21]. The FRLDM barriers of ^{213,215,217}Fr nuclei for $l = 0$ are obtained as 7.66, 7.90, and 8.12 MeV respectively. The ^{213}Fr nucleus is thus more unstable against fission compared to the other two Fr

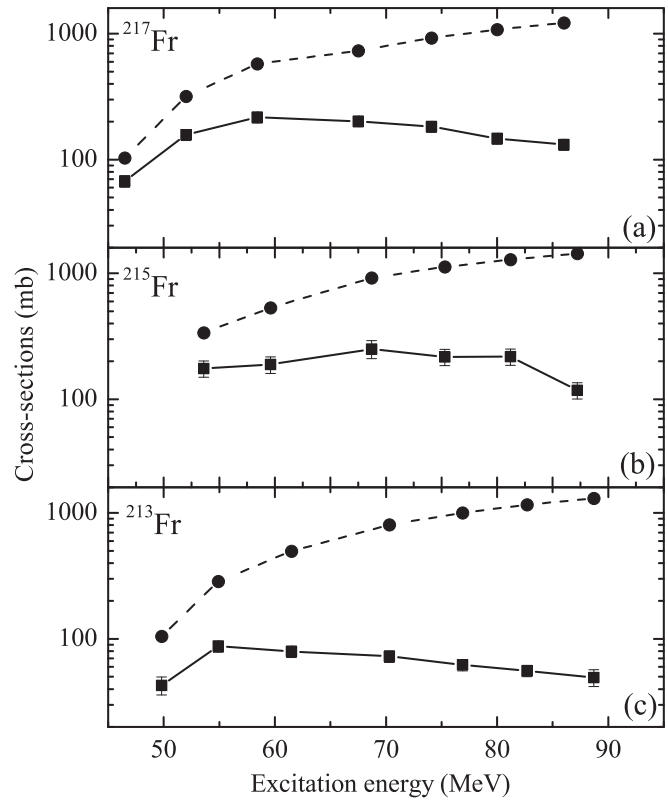

FIG. 4. (a)–(c) The excitation function of experimental ER cross sections (filled squares) along with the CCDEF predicted fusion cross section (filled circles) for different isotopes of Fr.

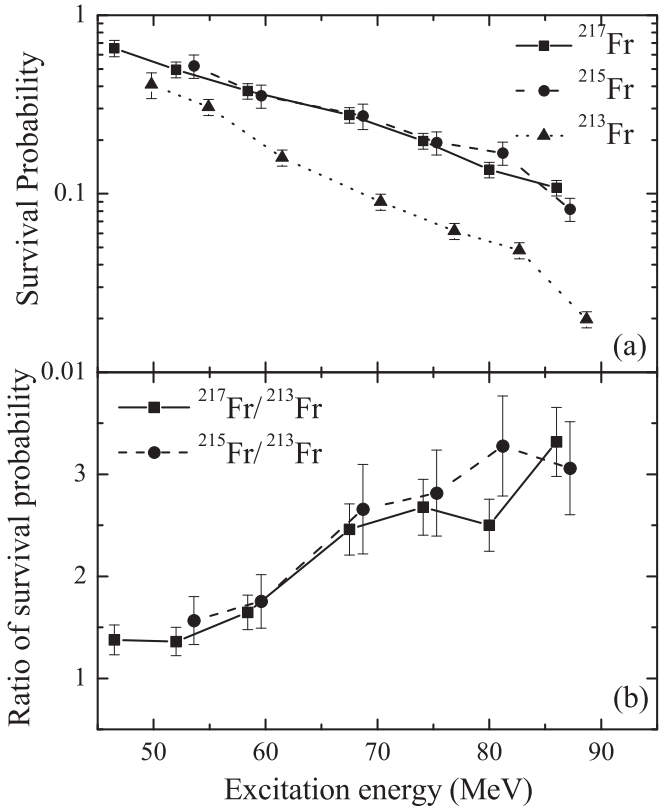

FIG. 5. (a) The excitation function of survival probability for different isotopes of Fr. (b) Ratio of survival probabilities of ^{217}Fr and ^{215}Fr with respect to ^{213}Fr. Lines are drawn to guide the eye.

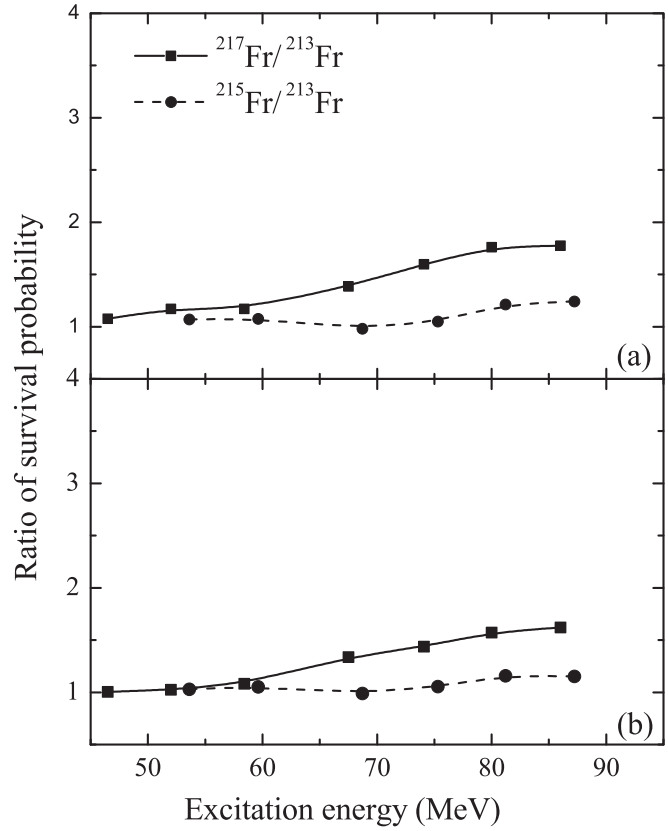

FIG. 6. (a) The ratio of survival probability of ^{217}Fr and ^{215}Fr with respect to ^{213}Fr using FRLDM fission barriers. (b) Same as in panel (a), using shell corrected FRLDM fission barriers.

isotopes according to the FRLDM potential, and the statistical model predictions of the ratio of the survival probability of ^{217}Fr and ^{215}Fr with respect to ^{213}Fr using the FRLDM fission barriers are shown in Fig. 6(a). When compared with the experimental trends given in Fig. 5(b), it is evident that the statistical model with FRLDM barriers grossly underestimates the ratios of the survival probabilities.

Following the suggestion by Aritomo [22], an excitation energy dependent shell correction is next applied to the FRLDM fission barriers. The parametrized form of the shell-corrected fission barrier for a CN with spin l is given as

$$V_B(l, E^*) = V_{\rm LDM}(l) - \Delta V_{\rm shl}(l) \tag{9}$$

with

$$\Delta V_{\rm shl}(l) = f_l \delta W \exp(-E^*/E_d), \tag{10}$$

where $V_{\rm LDM}(l)$ is the fission barrier at spin l from the FRLDM potential [21], E^* is the CN excitation energy, and E_d is the shell damping term [the same as used for the level density parameter in Eq. (7)]. Values between 14 and 18 MeV for E_d have been used earlier for hot fusion reactions [23]. We have introduced a scaling factor f_l in the shell correction term for the following reason: The shell correction to the fission barrier is obtained under the assumption that shell correction applies only to the ground-state mass and its effect at the saddle deformation is negligible [24]. This assumption implies that the saddle shape should be considerably deformed, which is true for very low spin compound nuclei. With increasing spin of a compound nucleus, the saddle configuration shifts to more compact shapes until the ground state and saddle configurations coincide and the FRLDM barrier vanishes. One would thus expect smaller values of the shell correction term as the saddle and the ground-state configurations come closer with increasing spin of the CN. This effect is taken into account by introducing the scaling factor f_l and a simple ansatz for it as $f_l = V_{\rm LDM}(l)/V_{\rm LDM}(0)$ is used in the present work.

Statistical model calculations are then performed using the shell corrected fission barriers. The calculated ratios of the survival probabilities of ^{217}Fr and ^{215}Fr with respect to ^{213}Fr are shown in Fig. 6(b). It is observed that the statistical model calculations with shell corrected fission barriers also considerably underpredict the ratios of experimental survival probabilities.

From the studies given above, it is evident that the FRLDM fission barriers obtained with or without shell correction cannot reproduce the relative survival probabilities of ^{217}Fr and ^{215}Fr nuclei with respect to ^{213}Fr. We therefore introduce a scaling factor k_f for the FRLDM barrier and treat it as an adjustable parameter to fit the experimental ER cross-sections. It may be mentioned here that in an earlier work [25] a shell correction term for the saddle configuration was added to the fission barrier in addition to the shell correction at the ground-state configuration. The strength of the shell correction at the saddle

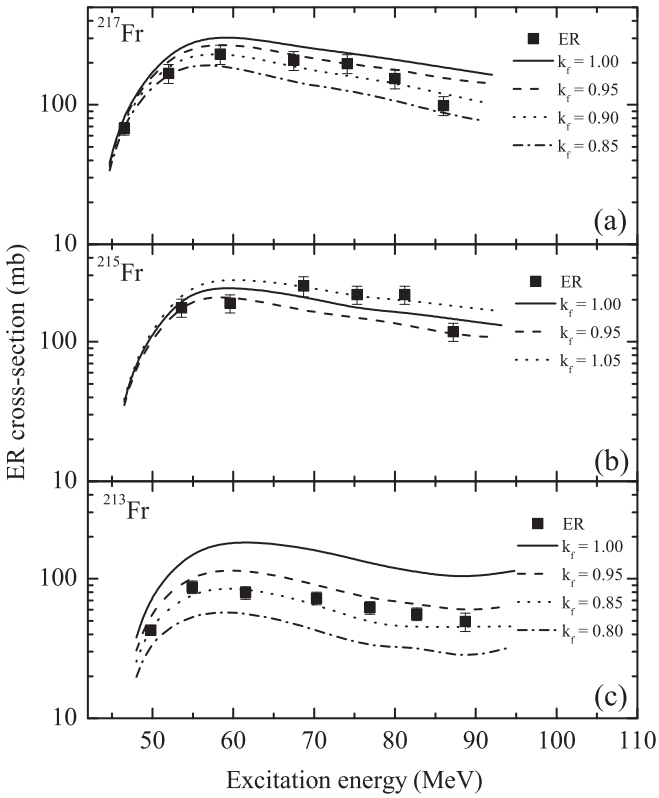

FIG. 7. (a)–(c) Experimental ER cross section (filled squares) for different isotopes of Fr along with the statistical model calculation results for different values of k_f using FRLDM fission barriers.

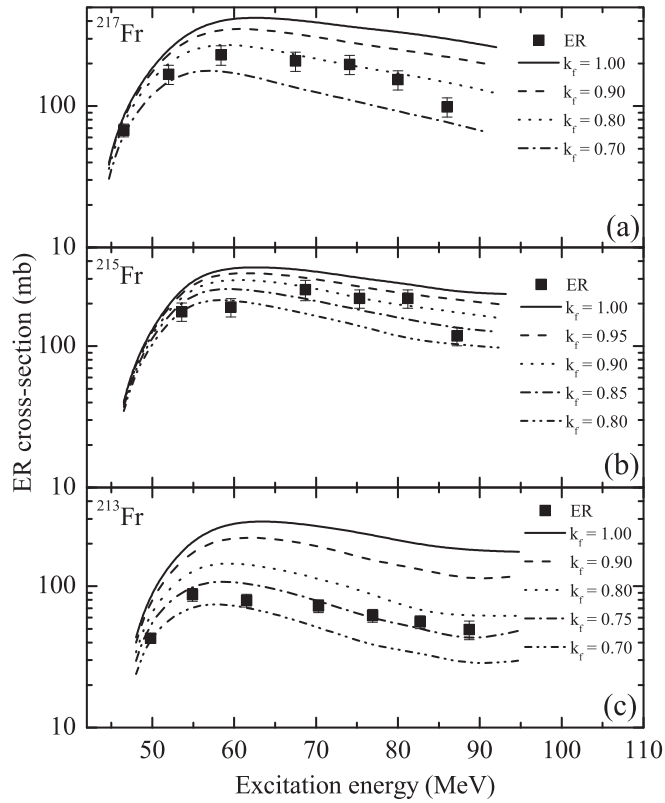

FIG. 8. (a)–(c) Experimental ER cross sections (filled squares) for different isotopes of Fr along with the statistical model calculation results for different values of k_f using shell corrected FRLDM fission barriers.

shape was treated as a free parameter to fit experimental data in Ref. [25]. However, we do not consider this term in the present work since we include a scaling factor for the FRLDM barrier. The fission barrier is now given as $V_B(l, E^*) = k_f V_{\rm LDM}(l) - \Delta V_{\rm shl}(l)$. We first perform statistical model calculations with different values of k_f without including the shell correction to the fission barriers. The calculated excitation functions are compared with the experimental ones in Fig. 7. It is observed that the ER cross sections for a given nucleus cannot be fitted with a single value of k_f though overall good fits to the ER excitation functions are obtained with $k_f = 0.9$, 1.0, and 0.85 for ^{217}Fr, ^{215}Fr, and ^{213}Fr compound nuclei respectively. The lowering of fission barrier is thus largest for ^{213}Fr.

Statistical model calculations are next carried out for different values of k_f with shell correction in the fission barrier as shown in Fig. 8. It is again observed that a single value of k_f cannot fit the ER cross sections over the entire range of excitation energies. Good overall fits to the ER excitation functions are obtained, however, with $k_f = 0.8$, 0.85, and 0.75 for ^{217}Fr, ^{215}Fr, and ^{213}Fr compound nuclei respectively. It may be noted here that the fitted k_f values obtained with shell correction in fission barriers are smaller than those obtained without shell correction. This is expected since shell correction terms for the nuclei under consideration increase the fission barriers and hence a stronger reduction of the FRLDM barriers are required to fit the experimental cross sections.

Lastly, we fit the experimental ER cross sections by varying the value of k_f at each excitation energy and obtain the excitation energy dependent values of k_f for each CN. The excitation energy dependence of k_f for all the three CN obtained with and without shell correction in fission barrier is given in Fig. 9. In both the cases, we find an increasing trend in k_f values with increase in excitation energy for all the three isotopes of Fr. We also note an isotopic dependence of k_f values where the scaling factor for ^{213}Fr has the lowest value at most of the excitation energies whereas its values for ^{215}Fr are the largest of the three nuclei. The present results therefore indicate a steeper fall in barrier height with decrease in neutron number than that predicted by the FRLDM for Fr isotopes with neutron numbers $\geqslant$126. A similar observation was made by Sagaidak *et al.* [4] for Po isotopes with neutron numbers $\leqslant$126. However, it may be remarked here that the same scaling factor is applied to the FRLDM barriers of all the daughter nuclei formed during the evaporation process and hence the fitted values of k_f reflect the combined effect of barrier scaling in all the nuclei in a decay chain and do not represent the best-fit barrier for the original CN in particular.

It may be noted in Fig. 9 that the excitation energy dependence of the scaling factor obtained with [Fig. 9(b)] and without [Fig. 9(a)] shell corrected fission barriers are very similar for the three Fr isotopes. This indicates that the excitation energy dependence of the shell correction term in fission barrier is not reflected in the excitation energy dependence of the scaling factor. One possible explanation

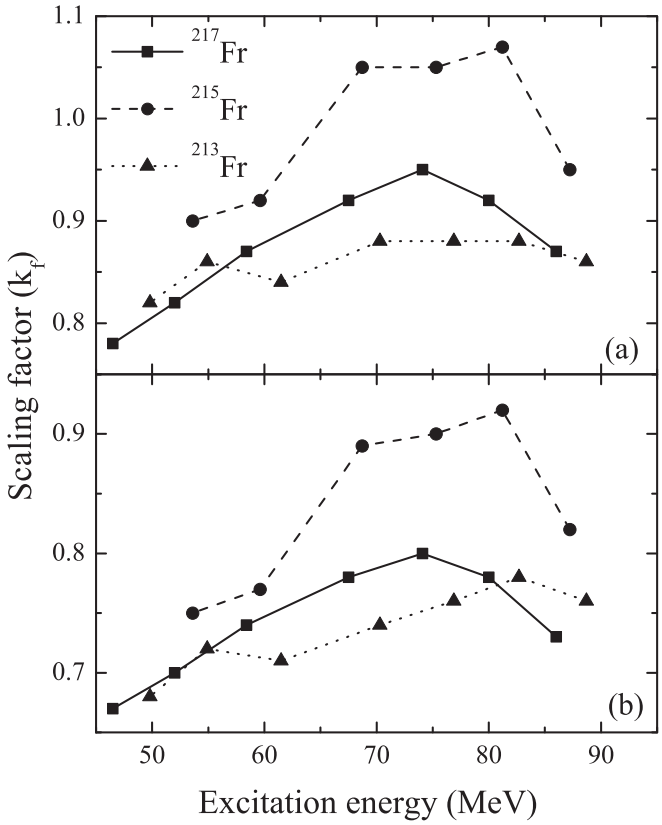

FIG. 9. (a) The best fit k_f obtained by fitting the experimental ER cross section with statistical model calculations using LDM fission barrier. (b) Same as in panel (a) using shell corrected fission barrier. Lines are drawn to guide the eye.

for the above observation is as follows: Most of the compound nuclei in the present study emit a number of neutrons before undergoing fission. Therefore fission takes place, on the average, at excitation energies which are substantially smaller than the initial compound nuclear excitation. For example, prescission neutron multiplicities for ^{213}Fr are 2.13, 3.37, and 4.71 at excitation energies of 55.3, 74, and 91.8 MeV, respectively [26]. This makes about 30–40 MeV of excitation energy available for fission over the entire range of initial compound nuclear excitation energies. Consequently the quenching of shell effect will be similar for compound nuclei at different initial excitation energies and hence no discernible excitation energy dependence due to shell effect is observed.

V. SUMMARY AND CONCLUSIONS

We have presented experimental evaporation residue cross-sectional data for the ^{19}F + ^{194,196,198}Pt reactions forming ^{213,215,217}Fr compound nuclei which are measured at excitation energies in the range of 50–90 MeV. Comparison of the survival probabilities of the compound nuclei derived from the experimental data shows that ^{213}Fr with $N = 126$ has lower stability against fission compared to ^{215}Fr and ^{217}Fr with neutron numbers $N = 128$ and 130 respectively.

Statistical model analysis of the ER cross sections shows that a scaling of the FRLDM fission barrier is necessary to fit the experimental data. An energy-dependent scaling factor is obtained by fitting the ER cross sections at each excitation energy. The fitted scaling factors for ^{213}Fr are found to be smaller than those of the other two nuclei for almost the entire range of excitation energies. This feature is clearly in disagreement with theoretical predictions where fission barriers for closed-shell nuclei are found to be larger than those of the neighboring non-closed-shell nuclei [27]. The reason for this discrepancy may lie in the neglect of collective excitation of level density in the saddle configuration in the present work and which can cause substantial loss of stability against fission [5]. This aspect requires further attention in future works.

ACKNOWLEDGMENTS

We thank the Pelletron and LINAC accelerator crew of IUAC, New Delhi, for providing beams of excellent quality throughout the experiment. The authors are grateful to A. Roy for his constant encouragement during the entire duration of the project. Thanks are also due to S. R. Abhilash for his help during target fabrication. The financial support from the Council of Scientific and Industrial Research (CSIR), government of India, in the form of a Shyama Prasad Mukherjee Research Grant (SPMF) to one of the authors (V.S.) is gratefully acknowledged. B.R.B. acknowledges the Department of Atomic Energy (DAE), government of India, for a DAE Young Scientist Research Grant (YSRA).

[1] Y. Oganessian, J. Phys. G: Nucl. Part. Phys. **34**, R165 (2007).
[2] B. B. Back, D. J. Blumenthal, C. N. Davids, D. J. Henderson, R. Hermann, D. J. Hofman, C. L. Jiang, H. T. Penttila, and A. H. Wuosmaa, Phys. Rev. C **60**, 044602 (1999).
[3] K. Mahata, S. Kailas, A. Shrivastava, A. Chatterjee, P. Singh, S. Santra, and B. S. Tomar, Phys. Rev. C **65**, 034613 (2002).
[4] R. N. Sagaidak and A. N. Andreyev, Phys. Rev. C **79**, 054613 (2009).
[5] A. R. Junghans, M. de Jong, H.-G. Clerc, A. V. Ignatyuk, G. A. Kudyaev, and K.-H. Schmidt, Nucl. Phys. A **629**, 635 (1998).
[6] D. Vermeulen, H.-G. Clerc, C.-C. Sahm, K.-H. Schmidt, J. G. Keller, G. Münzenberg, and W. Reisdorf, Z. Phys. A: At. Nucl. **318**, 157 (1984).
[7] G. Sawhney, G. Kaur, M. K. Sharma, and R. K. Gupta, Phys. Rev. C **88**, 034603 (2013).
[8] V. Singh, S. R. Abhilash, B. R. Behera, and D. Kabiraj, Nucl. Instr. Meth. A **635**, 20 (2011).
[9] N. Madhavan, I. Mazumdar, T. Varughese, J. Gehlot, S. Nath, D. A. Gothe, P. B. Chavan, G. Mohanto, M. B. Naik, I. Mukul, and A. K. Sinha, EPJ Web Conf. **17**, 14003 (2011).

[10] N. Madhavan, S. Nath, T. Varughese, J. Gehlot, A. Jhingan, P. Sugathan, A. K. Sinha, R. Singh, K. M. Varier, M. C. Radhakrishna, E. Prasad, S. Kalkal, G. Mohanto, J. J. Das, R. Kumar, R. P. Singh, S. Muralithar, R. K. Bhowmik, A. Roy, Rajesh Kumar, S. K. Suman, A. Mandal, T. S. Datta, J. Chacko, A. Choudhury, U. G. Naik, A. J. Malyadri, M. Archunan, J. Zacharias, S. Rao, Mukesh Kumar, P. Barua, E. T. Subramaniam, K. Rani, B. P. Ajith Kumar, and K. S. Golda, PRAMANA J. Phys. **75**, 317 (2010).
[11] J. Sarén, J. Uusitalo, M. Leino, and J. Sorri, Nucl. Instrum. Methods A **654**, 508 (2011).
[12] S. Nath, Comput. Phys. Commun. **180**, 2392 (2009).
[13] E. Prasad, K. M. Varier, N. Madhavan, S. Nath, J. Gehlot, S. Kalkal, J. Sadhukhan, G. Mohanto, P. Sugathan, A. Jhingan, B. R. S. Babu, T. Varughese, K. S. Golda, B. P. Ajith Kumar, B. Satheesh, S. Pal, R. Singh, A. K. Sinha, and S. Kailas, Phys. Rev. C **84**, 064606 (2011).
[14] P. Fröbrich and I. I. Gontchar, Phys. Rep. **292**, 131 (1998).
[15] N. Bohr and J. A. Wheeler, Phys. Rev. **56**, 426 (1939).
[16] V. M. Strutinsky, Phys. Lett. B **47**, 121 (1973).
[17] A. Bohr and B. R. Mottelson, *Nuclear Structure*, Vol. I (Benjamin Press, New York, 1969).
[18] A. V. Ignatyuk, G. N. Smirenkin, and A. S. Tishin, Sov. J. Nucl. Phys. **21**, 255 (1975).
[19] W. Reisdorf, Z. Phys. A **300**, 227 (1981).
[20] J. Fernandez Niello, C. H. Dasso, and S. Landowne, Comput. Phys. Commun. **54**, 409 (1989).
[21] A. J. Sierk, Phys. Rev. C **33**, 2039 (1986).
[22] Y. Aritomo, Nucl. Phys. A **780**, 222 (2006).
[23] M. G. Itkis, Y. T. Oganessian, and V. I. Zagrebaev, Phys. Rev. C **65**, 044602 (2002).
[24] W. D. Myers and W. J. Swiatecki, Nucl. Phys. A **601**, 141 (1996).
[25] K. Mahata, S. Kailas, and S. S. Kapoor, Phys. Rev. C **74**, 041301(R) (2006).
[26] V. Singh, B. R. Behera, M. Kaur, A. Kumar, P. Sugathan, K. S. Golda, A. Jhingan, M. B. Chatterjee, R. K. Bhowmik, D. Siwal, S. Goyal, J. Sadhukhan, S. Pal, A. Saxena, S. Santra, and S. Kailas, Phys. Rev. C **87**, 064601 (2013).
[27] P. Moller, A. J. Sierk, T. Ichikawa, A. Iwamoto, R. Bengtsson, H. Uhrenholt, and S. Aberg, Phys. Rev. C **79**, 064304 (2009).